



## Doped ceria anode interlayer for low-temperature solid oxide fuel cells with nanothin electrolyte



Sanghoon Ji<sup>a</sup>, Yoon Ho Lee<sup>b</sup>, Taehyun Park<sup>b</sup>, Gu Young Cho<sup>b</sup>, Seungtak Noh<sup>b</sup>, Yeageun Lee<sup>b</sup>, Minwoo Kim<sup>c</sup>, Seungbum Ha<sup>b</sup>, Jihwan An<sup>d,\*</sup>, Suk Won Cha<sup>a,b,\*\*</sup>

<sup>a</sup> Graduate School of Convergence Science and Technology, Seoul National University, 864-1 Iui-dong, Yeongtong-gu, Suwon 443-270, South Korea

<sup>b</sup> Department of Mechanical and Aerospace Engineering, Seoul National University, 1 Gwanak-ro, Gwanak-gu, Seoul 151-742, South Korea

<sup>c</sup> Creative and Fundamental Research Division, Korea Electrotechnology Research Institute, Changwon 642-120, South Korea

<sup>d</sup> Manufacturing Systems and Design Engineering Programme, Seoul National University of Science and Technology, 232 Gongneung-ro, Nowon-gu, Seoul 139-743, South Korea

### ARTICLE INFO

Available online 10 May 2015

#### Keywords:

Gadolinium-doped ceria  
Anode interlayer  
Nanothin electrolyte  
Radio frequency sputtering  
Solid oxide fuel cell

### ABSTRACT

Gadolinium-doped ceria (GDC) deposited by radio frequency magnetron sputtering is utilized as the anode interlayer for low-temperature solid oxide fuel cells (LT-SOFCs) with a nanothin yttria-stabilized zirconia (YSZ) electrolyte and Ni/Pt electrodes. When the thickness ratio of YSZ electrolyte versus 100 nm GDC anode interlayer is at or below 1.5, the electrochemical performance of the LT-SOFC is severely poor due to the microstructural instability of the GDC anode interlayer under high-temperature reducing atmospheric conditions. At 500 °C, the peak power density of the LT-SOFC with a Ni anode and a 20 nm GDC anode interlayer is ~30% higher than that without the GDC anode interlayer due to faster reaction kinetics on the anode side.

© 2015 Elsevier B.V. All rights reserved.

## 1. Introduction

Doped ceria is considered as the promising electrolyte material for solid oxide fuel cells (SOFCs) due to its high oxygen-ion conductivity, superior oxygen surface exchange coefficient at the cathode side interface, and, therefore, excellent functionality as an interlayer between doped zirconia electrolyte and Co-containing perovskite cathode [1–7]. Furthermore, electronically and catalytically active characteristics of doped ceria under high-temperature reducing atmosphere improves the anode reaction kinetics when inserted between the anode and the electrolyte, and resultantly the electrochemical performance of SOFCs further improves [8,9]. On the other hand, it is known that the structural stability of ceria under reducing atmosphere is poor due to the structural change of ceria from CeO<sub>2</sub> to Ce<sub>2</sub>O<sub>3</sub> [10], which has often prevented the doped ceria from being widely utilized for SOFCs.

Generally, porous micro-structured cermet has been utilized to obtain the sufficient density of triple phase boundary that is the site where electrode, electrolyte, and gas meet at the anode side of SOFCs [8,11]. However, cermet comprised of ceramic and oxidized metal particles requires sintering processes at high-temperature (above 1000 °C) for low ohmic resistance, which incurs complex manufacturing, metal agglomeration, and second phase formation issues [12,13].

These disadvantages require the development of anode structures with dense triple phase boundary and, simultaneously, without sintering processes. As a representative example, the gadolinium-doped ceria (GDC)-impregnated Ni anode structure demonstrated by Jiang et al. did not need sintering processes while remarkably lowering anode overpotential [14]. Nevertheless, such a strategy has never been applied to SOFCs with nanothin doped-zirconia electrolytes operating at low-temperature (below 500 °C) [15].

In this study, the anode structure with no-sintering process and fast anode reaction kinetics was fabricated with a form of metal-ceramic bilayer, and was applied to the low-temperature SOFC (LT-SOFC) with nanothin doped zirconia electrolyte. The structural property of reduced GDC thin film was characterized, and the microstructural instability of GDC anode interlayer was electrochemically evaluated using SOFCs with various electrolyte configurations. The 20 nm GDC anode interlayer, which was adopted by consideration of its microstructural stability, enhanced the electrochemical performance through fast anode reaction kinetics under reducing atmosphere. The result presented in this paper has implications in improving the performance of nanothin electrolyte SOFCs at low-temperature regime.

## 2. Experimental methods

### 2.1. Thin film fabrication

For electrolyte deposition, GDC thin films were deposited using a commercial sputtering machine (A-Tech System Ltd., Korea) with a customized rotation unit. Target to substrate distance was 75 mm, a

\* Corresponding author. Tel.: +82 2 970 7276; fax: +82 2 974 5388.

\*\* Correspondence to: S.W. Cha, Graduate School of Convergence Science and Technology, Seoul National University, 864-1 Iui-dong, Yeongtong-gu, Suwon 443-270, South Korea. Tel.: +82 2 880 8050; fax: +82 2 880 1696.

E-mail addresses: [jihwanan@seoultech.ac.kr](mailto:jihwanan@seoultech.ac.kr) (J. An), [swcha@snu.ac.kr](mailto:swcha@snu.ac.kr) (S.W. Cha).

substrate support was rotated at 4 rpm to reduce the growth rate deviation. Sputtering gas was a mixture of Ar and O<sub>2</sub> in the volumetric ratio of 80:20. Background pressure was kept at 1.3 Pa during deposition. Radio frequency magnetron power of a sputtering gun was 50 W, GDC disk pellet with a 10 mol% Gd<sub>2</sub>O<sub>3</sub> was used as the target. Sputtered yttria-stabilized zirconia (YSZ) thin films were deposited under same processing conditions with YSZ disk pellet with an 8 mol% Y<sub>2</sub>O<sub>3</sub>. The fabrication process of conformal YSZ thin film is presented in our previous work [16]. For electrode deposition, a 99.99% purity Pt and a 99.99% purity Ni target were used to deposit Pt thin films and Ni thin films, respectively, with direct current power of 200 W in 99.9999% purity Ar atmosphere. Background pressure was kept at 0.7 and 12 Pa for dense and porous microstructure, respectively.

## 2.2. Thin film characterization

The crystalline property of thin film was investigated by X-ray diffraction (XRD) using X'Pert Pro (PANalytical, Netherland) with Cu K $\alpha$  radiation in the grazing incidence scan mode with a step size of 0.02°. The surface microstructure of thin film was analyzed by focused ion beam and field emission scanning electron microscopy (FIB/FE-SEM) operated at 5 kV using the quanta 3D FEG (FEI Company, Netherland) instrument. The surface morphology of thin film was examined by atomic force microscopy (AFM) using the XE 100 (Park Systems, Korea) instrument. Non-contact mode AFM scanning herein was carried using silicon tips with a ~10 nm radius, the scan dimension was 10  $\mu$ m  $\times$  10  $\mu$ m. High angle annular dark field scanning transmission electron microscopy (HAADF-STEM) and energy-dispersive X-ray spectroscopy (EDX) in STEM mode were conducted to investigate the nanostructure and local composition, respectively, using the JEOL-2100F (JEOL, Japan) under an accelerating voltage of 200 keV.

## 2.3. Electrochemical evaluation

Commercial anodic aluminum oxide (AAO, Synkera, USA) templates, Al foil anodized in an acid solution to form well-arrayed nanopores, with the thickness of 100  $\mu$ m and the pore size of 80 nm were used as the porous supporter for LT-SOFCs. The physical mask for the opening area of 1 mm<sup>2</sup> was comprised of a square-patterned 0.1 mm thick stainless steel (SS) plate (lower layer) and a thicker SS plate pressing the lower plate (upper layer). Test cells were attached to the custom-made H<sub>2</sub> feeding chamber using a ceramic adhesive (CP4010, Aremco Products, Inc., USA), which were heated to 500 °C with a ramping rate of 10 °C/min using halogen heaters. 50 sccm dry H<sub>2</sub> gas was supplied to the anode side and the cathode was exposed to the atmospheric environment. Electrochemical measurements were carried out after exposure to H<sub>2</sub> for 1 h at the anode. The anode was connected with a combination of silver paste (597A, Aremco Products, Inc., USA) and a 0.5 mm diameter silver wire while the cathode was contacted using a hardened-steel with a radius of 0.19 mm probe moved by a XYZ stage. Polarization curves and electrochemical impedance spectroscopy (EIS) measurements of test cells were measured using an electrochemical testing system (1287/1260, Solatron Analytical, UK). The anode was selected as the counter electrode which was connected to the reference electrode, and the cathode functioned as the working electrode. During the EIS measurements, the alternating voltage with an amplitude of 50 mV was applied to the cathode with respect to the anode.

## 3. Results and discussion

### 3.1. Instability of GDC anode interlayer under reducing atmosphere

Despite the weak structural stability of doped ceria under reducing atmosphere, the feasibility of doped ceria as single-electrolytes for low-temperature SOFCs was reported by several groups according to the fact that ceria reduction at temperatures below 500 °C is only limited to the electrolyte surface or thereabouts [1,15]. In this regard, researches aiming

at the use of nanothin doped ceria as single-electrolytes were recently carried out to further reduce the operating temperature of SOFCs [16,17]. However, nanothin doped ceria single-electrolytes exposed to reducing atmosphere generated considerably low open circuit voltage (below 0.7 V) and the vastly insufficient peak power density by the ceria reduction as well as the gas permeation through the electrolyte. This investigation implies that the thermal stability of the doped ceria needs to be considered as an important factor when nanothin GDC is employed as the anode interlayer.

Using XRD analysis, we confirmed the 2-theta values for 80 nm GDC film treated in H<sub>2</sub> atmosphere (50 sccm dry H<sub>2</sub>) are slightly lower than those treated in air atmosphere (50 sccm air) at 500 °C for 2 h (Fig. 1), which is likely due to the increase of lattice parameter by the increase of oxygen vacancy concentration [7,18]. Based on the fact that a change in structural property of thin film can also have a noticeable impact on its microstructural characteristics [19], we tried to examine the effects of the reduction on the mechanical stability using various-configured electrolyte cells. Although this approach could seem to be an indirect way to verify such effects, the approach has been previously shown to be sensitive enough to reflect the electrolyte integrity [20]. Fig. 2(a) and (b) show the electrolyte type and electrochemical performance of the tested cells, respectively. The 100 nm GDC single-electrolyte cell (Cell 1) shows zero open circuit voltage (OCV) with the ohmic resistance of ~0.001  $\Omega$  cm<sup>2</sup>. Because this result may be due to several different factors such as ceria reduction and/or electrode material diffusion through the grain-boundaries of the columnar GDC electrolyte, it was difficult to figure out the microstructural stability of the GDC from this result only. We, therefore, additionally prepared 4 cells with varying electrolyte configurations in which a conformal and dense YSZ electrolyte layer deposited via atomic layer deposition is located on the cathode side. First, 150 nm single-conformal YSZ electrolyte cell (Cell 2) generates the OCV of ~1.16 V, which means the conformal YSZ layer is sufficiently insulative on electronic conduction. Next, the conformal YSZ electrolyte layers with different thicknesses, i.e., 150 nm (Cell 3), 100 nm (Cell 4), and 50 nm (Cell 5) in thickness, were deposited on the GDC anode interlayer (100 nm thick). The OCVs and the peak power densities of cells 3–5 are observed to be significantly lower than those of the cell 2. Also among the cells 3–5, the OCV and the peak power density decrease notably as the YSZ layer becomes thinner. We think this is because nanothin GDC anode interlayer under high-temperature and strong reducing atmospheric conditions becomes unstable in terms of microstructure. In result, the density of microstructural defects in YSZ layers on the GDC layer may also increase. This argument is supported by the HAADF-STEM analysis result showing the appearance of voids (black area) in a few tens of nanometer size in the GDC anode interlayer (Fig. 2c). Resultantly, this consideration

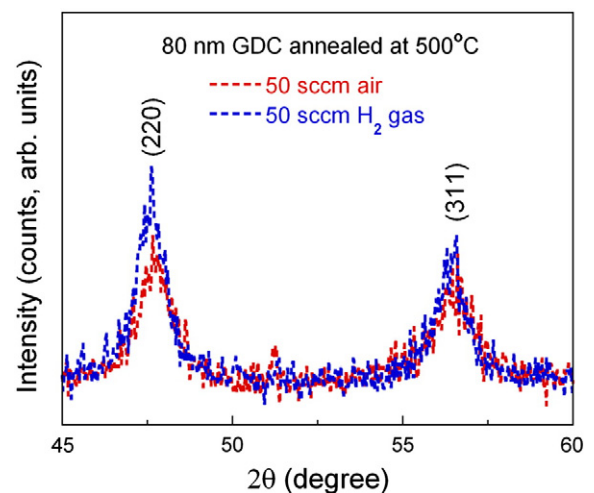
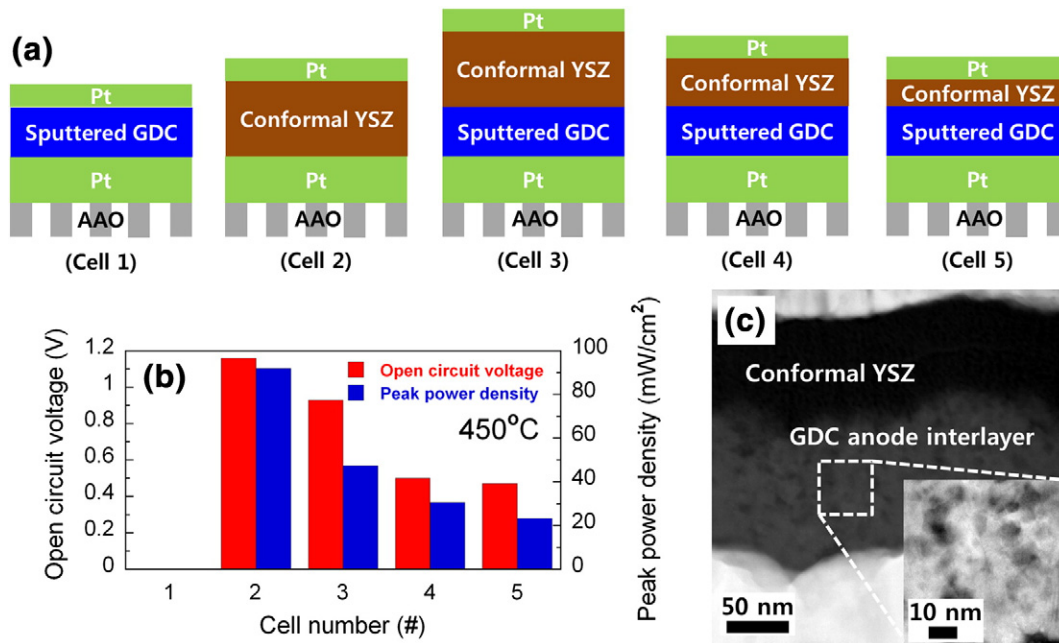


Fig. 1. X-ray diffractometry results for 80 nm gadolinium-doped ceria (GDC) films after oxidation and reduction processes at 500 °C for 2 h.



**Fig. 2.** (a) Schematic presentation of anodic aluminum oxide (AAO)-supported cells with different electrolyte configuration, (b) their open circuit voltage and peak power density, at 450 °C, and (c) high angle annular dark field scanning transmission electron microscopy (HAADF-STEM) images of AAO-supported cell with a GDC anode interlayer (lower side) and a 100 nm conformal yttria-stabilized zirconia layer (YSZ) (upper side) at different magnifications.

could present the necessity to significantly decrease the thickness of GDC anode interlayer compared to that of YSZ electrolyte.

### 3.2. Effects of GDC anode interlayer on electrochemical performance

To verify the effects of GDC anode interlayer (20 nm thick) on electrochemical performance, LT-SOFCs without and with the GDC anode interlayer (called to Cell-A and Cell-B, respectively) were fabricated via sputtering. Fig. 3a shows FE-SEM top-view images for 400 nm Ni-AAO (left side) and 400 nm Ni-AAO coated with 20 nm GDC anode interlayer (right side). The GDC anode interlayer was deposited in

granular structure, which led to the slight increase of the surface roughness: AFM scanning revealed that root mean square roughnesses for Ni-AAO and Ni-AAO with GDC anode interlayer are 21 nm and 25 nm, respectively. Fig. 3b shows the cross-sectional HAADF-STEM image of the Cell-B (200 nm porous Pt cathode/500 nm dense YSZ/20 nm GDC anode interlayer/400 nm Ni dense anode) (Fig. 3b). HAADF-STEM imaging and EDX mapping results of the dashed rectangular region of Fig. 3(b) confirms that 20 nm GDC interlayer is uniformly positioned between the Ni anode and the YSZ electrolyte (Fig. 3c).

EIS spectra obtained at different bias voltages (OCV and 0.5 V) for Cell-B are compared to identify the resistances associated with each of

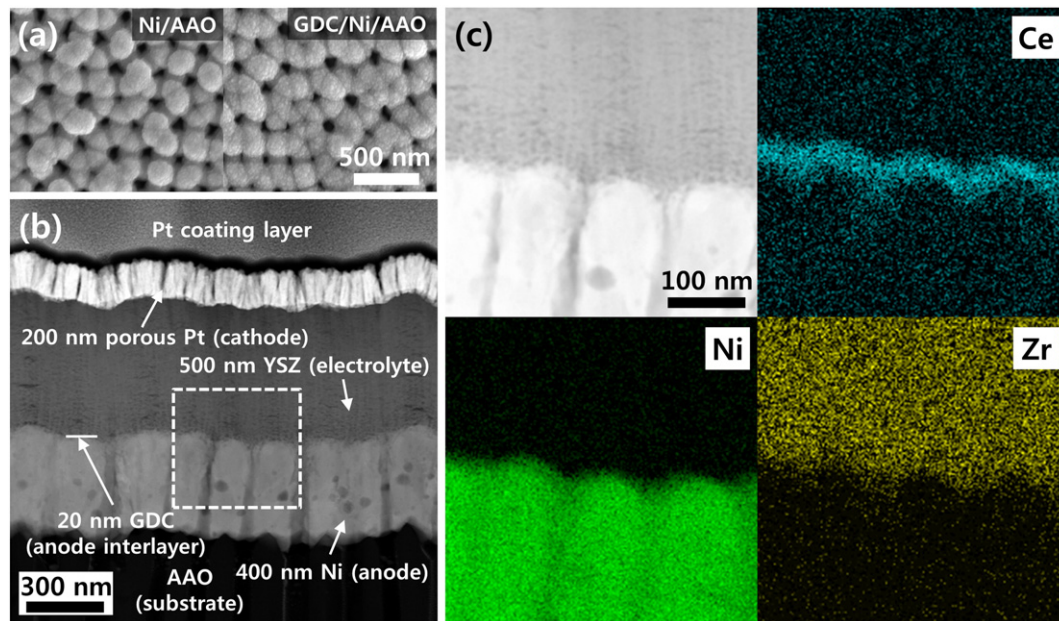


**Fig. 3.** (a) Field emission scanning electron microscopy top-view images for 400 nm Ni (left side) and 20 nm gadolinium-doped ceria (GDC) deposited on 400 nm Ni (right side) on AAO substrate, (b) HAADF-STEM image of AAO-supported YSZ electrolyte cell with a 20 nm GDC anode interlayer and a 200 nm porous Pt cathode, and (c) enlarged image in the dashed rectangular region in Fig. 3(b) and energy-dispersive X-ray spectroscopy mappings for main component elements in the same region.

the arcs [21,22]. Totally, three arcs are shown: there is one overlapping arc in high frequency regime (with a time constant of  $\sim 500$  kHz) (Fig. 4a), which indicates this arc originates from ohmic process. In the meantime, two more arcs in medium frequency regime (with a time constant of  $\sim 50$  Hz) and in low frequency regime (with a time constant of  $\sim 2$  Hz), which we think are associated with activation process (anode/cathode) and mass transport process, respectively. Fig. 4b shows the EIS spectra for Cell-A and Cell-B at OCV. The low frequency arc for Cell-B diverges below 2 Hz, contrary to Cell-A, which is likely to be due to Warburg effects generally appearing in such a low frequency regime ( $< 10$  Hz) [23,24]. Because previously demonstrated SOFCs having identical electrode layers without doped ceria anode interlayer did not show any notable low frequency divergence of EIS spectra under identical characterization conditions, we think these Warburg effects mainly originate from poor mass transport on the anode side [20–22,25]. Likewise, this argument corresponds well to the previous study in which doped ceria anode interlayer resulted in poor mass transport caused by sluggish gas diffusion through the doped ceria anode interlayer [8]. Least-square fitting of the medium frequency arc (with a time constant of 50 Hz) for Cell-B was conducted to distinguish anode and cathode/electrolyte interfacial resistances, which were  $0.6 \Omega \text{ cm}^2$  and  $6.3 \Omega \text{ cm}^2$ , respectively. For Cell-A, the size of the medium frequency arc was  $12.8 \Omega \text{ cm}^2$ , among which the cathode/electrolyte interfacial resistance can be estimated to be  $6.3 \Omega \text{ cm}^2$  because Cell-A and Cell-B have same cathode reaction kinetics. Therefore, the difference ( $5.9 \Omega \text{ cm}^2$ ) in the size of the medium frequency arc between Cell-A and Cell-B can be considered to come from the difference in anode activation process. The faster anode reaction kinetics for Cell-B than Cell-A can be accounted for based on two

phenomenological understandings: 1) there may be more catalytically active sites (or longer triple phase boundary length) on the anode side due to the infiltration of GDC into Ni anode [8], or 2) the GDC may offer higher surface exchange rate at the anode side [26]. On the other hand, the high frequency intercept ( $0.36 \Omega \text{ cm}^2$ ) of Cell-B is slightly higher than that ( $0.31 \Omega \text{ cm}^2$ ) of Cell-A. Because the ionic resistance for two kinds of cells is almost same [20,22], we think that Cell-B has the relatively low current collecting performance compared to Cell-A [27]. The possible reason for this is that the GDC anode interlayer may provide insufficient electron-conducting paths, in spite of being electronically activated under high-temperature reducing atmosphere, resulting in higher ohmic resistance. The size of the high frequency arc ( $0.57 \Omega \text{ cm}^2$ ) with a time constant of 500 kHz for Cell-B is slightly bigger than that ( $0.41 \Omega \text{ cm}^2$ ) for Cell-A, which is likely to be due to the increase of thickness and grain-boundary density of the electrolyte by the insertion of GDC anode interlayer.

Fig. 4c show polarization curves for two kinds of cells. The OCV of Cell-B is 1.15 V, which is very close to the theoretical value (1.17 V) at the operating conditions [24]. With increasing the current density, the difference in voltage drop becomes bigger between Cell-A and Cell-B. Resultantly, the peak power density of the Cell-B is  $\sim 30\%$  higher than that of the Cell-A. The polarization curve for Cell-B reflects negative effects relative to mass transport above  $400 \text{ mA/cm}^2$ , i.e., shows a steeper voltage drop at high current density region [16], which is parallel with the aforementioned interpretation of relevant EIS results. Exchange current densities for Cell-A and for Cell-B estimated from Tafel plots are  $1.27 \text{ A/cm}^2$  and  $1.73 \text{ A/cm}^2$ , respectively, which supports that Cell-B shows faster reaction kinetics on the anode side than Cell-A (Fig. 4d). Meanwhile the OCV of Cell-B was retained at

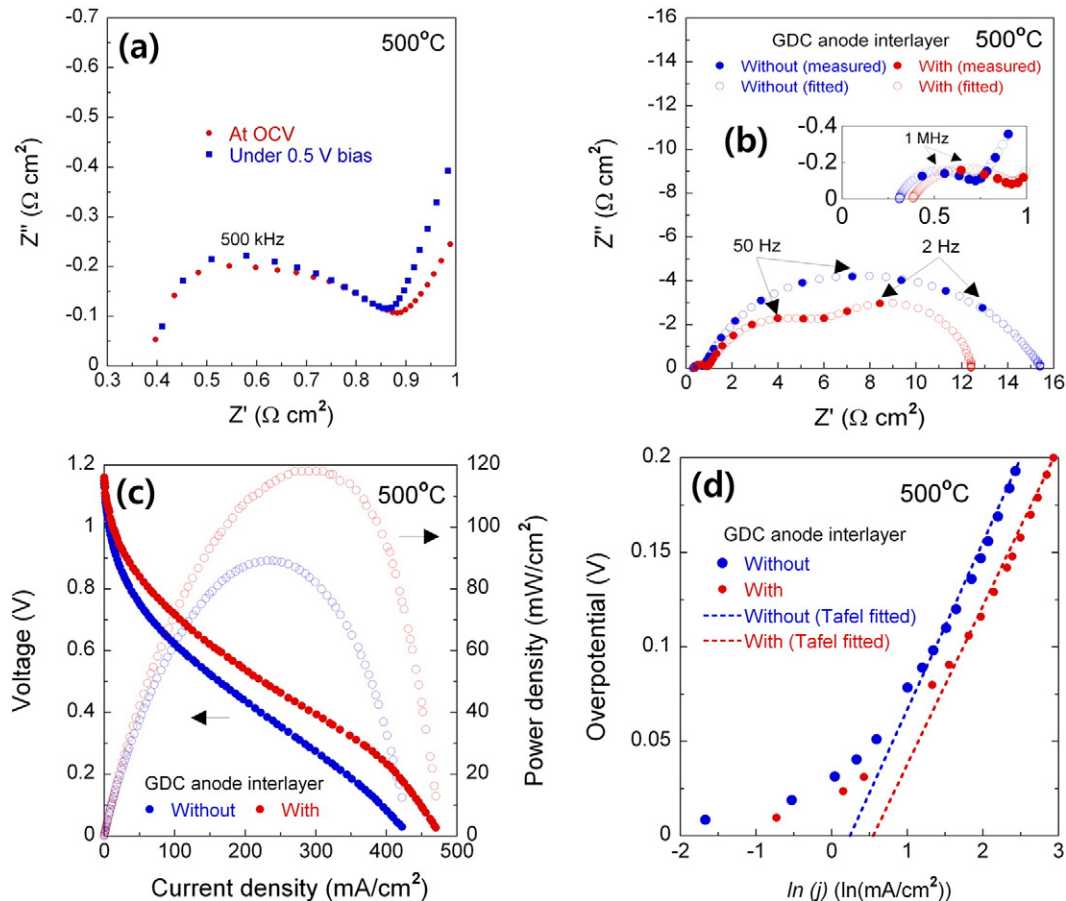


Fig. 4. (a) Electrochemical impedance spectroscopy (EIS) bias study for the AAO-supported YSZ electrolyte cell with a 20 nm GDC anode interlayer, (b) EIS results, (c) polarization curves, and (d) their Tafel plots for the AAO-supported YSZ electrolyte cells with and without a 20 nm GDC anode interlayer, at 500 °C.

~1.15 V for 5 h at the operating temperature of 500 °C, meaning that the insertion of 20 nm thick of GDC anode interlayer rarely affects the microstructural-stability of the electrolyte.

#### 4. Conclusion

We showed that the doped ceria anode interlayer of a few tens of nanometers thickness inserted between the metal anode and the nanothin doped zirconia electrolyte enhances the performance of LT-SOFCs operated with hydrogen fuel at the anode. When 500 nm YSZ electrolyte is used, the LT-SOFC with 20 nm doped ceria anode interlayer generates a ~30% higher peak power density than the LT-SOFC without the doped ceria anode interlayer due to faster reaction kinetics on the anode side. Furthermore, it was confirmed that the low microstructural stability of doped ceria under reducing condition could result in the poor electrochemical performance of LT-SOFCs when the ratio of YSZ thickness to GDC thickness becomes less than 1.5 (YSZ: 150 nm, GDC: 100 nm). Consequently, the applicability of the doped ceria presents the methodology to improve anode reaction kinetics for LT-SOFCs. Also careful consideration on the thickness of doped ceria anode interlayer and conformal YSZ electrolyte may suggest strategies in enhancing the output power and simultaneously ensuring the microstructural stability in LT-SOFCs.

#### Acknowledgement

This research was partially supported by the National Research Foundation of Korea (NRF) grant funded by the Korea government (2013R1A1A2A10065234).

#### References

- [1] B.C.H. Steele, A. Heinzel, Materials for fuel-cell technologies, *Nature* 414 (2001) 345.
- [2] G. Constantin, C. Rossignol, P. Briois, A. Billard, L. Dessemond, E. Djurado, Efficiency of a dense thin CGO buffer layer for solid oxide fuel cell operating at intermediate temperature, *Solid State Ionics* 249–250 (2013) 98.
- [3] S. Sønderby, T. Klemensø, B.H. Christensen, K.P. Almtoft, J. Lu, L.P. Nielsen, P. Eklund, Magnetron sputtered gadolinia-doped ceria diffusion barriers for metal-supported solid oxide fuel cells, *J. Power Sources* 267 (2014) 452.
- [4] S.-Y. Park, J.H. Ahn, C.-W. Jeong, C.W. Na, R.-H. Song, J.-H. Lee, Ni-YSZ-supported tubular solid oxide fuel cells with GDC interlayer between YSZ electrolyte and LSCF cathode, *Int. J. Hydrog. Energy* 39 (2014) 12894.
- [5] S. Sønderby, P.L. Pop, J. Lu, B.H. Christensen, K.P. Almtoft, L.P. Nielsen, P. Eklund, Strontium diffusion in magnetron sputtered gadolinia-doped ceria thin film barrier coatings for solid oxide fuel cells, *Adv. Energy Mater.* 3 (2013) 923.
- [6] D. Roehrens, F. Han, M. Haydn, W. Schafbauer, D. Sebold, N.H. Menzler, H.P. Buchkremer, Advances beyond traditional SOFC cell designs, *Int. J. Hydrog. Energy* (2015) <http://dx.doi.org/10.1016/j.ijhydene.2015.01.155>.
- [7] N. Mahato, A. Banerjee, A. Gupta, S. Omar, K. Balani, Progress in material selection for solid oxide fuel cell technology: A review, *Prog. Mater. Sci.* (2015) <http://dx.doi.org/10.1016/j.pmatsci.2015.01.001>.
- [8] T. Tsai, S.A. Barnett, Effect of mixed-conducting interfacial layers on solid oxide fuel cell anode performance, *J. Electrochem. Soc.* 145 (1998) 1696.
- [9] T. Horita, K. Yamaji, N. Sakai, M. Ishikawa, H. Yokokawa, M. Dokiya, Electrode reaction at platinum/ceria surface modified YSZ interface, *Ionics* 3 (1997) 67.
- [10] H.J. Ko, J.-J. Lee, S.-H. Hyun, Structural stability of the GDC electrolyte for low temperature SOFCs depending on fuels, *Electrochem. Solid-State Lett.* 13 (2010) B113.
- [11] M.B. Kakade, S. Ramanathan, D. Das, Gel-combustion, characterization and processing of porous Ni-YSZ cermet for anodes of solid oxide fuel cells (SOFCs), *Ceram. Int.* 37 (2011) 195.
- [12] A. Infortuna, A.S. Harvey, U.P. Muecke, L.J. Gauckler, Nanoporous Ni-CeO<sub>0.8</sub>Gd<sub>0.2</sub>O<sub>1.9-x</sub> thin film cermet SOFC anodes prepared by pulsed laser deposition, *Phys. Chem. Chem. Phys.* 11 (2009) 3663.
- [13] S.P. Jiang, Y.Y. Duan, J.G. Love, Fabrication of high-performance Ni/Y<sub>2</sub>O<sub>3</sub>-ZrO<sub>2</sub> cermet anodes of solid oxide fuel cells by ion impregnation, *J. Electrochem. Soc.* 149 (2002) A1175.
- [14] S.P. Jiang, S. Zhang, Y.D. Zhen, A.P. Koh, Performance of GDC-impregnated Ni anodes of SOFCs, *Electrochem. Solid-State Lett.* 7 (2004) A282.
- [15] S. Zha, A. Moore, H. Abernathy, M. Liu, GDC-based low-temperature SOFCs powered by hydrocarbon fuels, *J. Electrochem. Soc.* 151 (2004) A1128.
- [16] S. Ji, I. Chang, Y.H. Lee, J. Park, J.Y. Paek, M.H. Lee, S.W. Cha, Fabrication of low-temperature solid oxide fuel cells with a nanothin protective layer by atomic layer deposition, *Nanoscale Res. Lett.* 8 (2013) 48.
- [17] D.-H. Myung, J. Hong, K. Yoon, B.-K. Kim, H.-W. Lee, J.-H. Lee, J.-W. Son, The effect of an ultra-thin zirconia blocking layer on the performance of a 1- $\mu$ m-thick gadolinia-doped ceria electrolyte solid-oxide fuel cell, *J. Power Sources* 206 (2012) 91.
- [18] Y. Wang, K. Duncan, E.D. Wachsman, F. Ebrahimi, The effect of oxygen vacancy concentration on the elastic modulus of fluorite-structured oxides, *Solid State Ionics* 178 (2007) 53.
- [19] Y. Li, P.-C. Su, L.M. Wong, S. Wang, Chemical stability study of nanoscale thin film yttria-doped barium cerate electrolyte for micro solid oxide fuel cells, *J. Power Sources* 268 (2014) 804.
- [20] S. Ji, I. Chang, Y.H. Lee, M.H. Lee, S.W. Cha, Performance enhancement of thin-film ceramic electrolyte fuel cell using bi-layered yttrium-doped barium zirconate, *Thin Solid Films* 539 (2013) 117.
- [21] W. Yu, S. Ji, G.Y. Cho, S. Noh, W.H. Tanveer, J. An, S.W. Cha, Atomic layer deposition of ultrathin blocking layer for low-temperature solid oxide fuel cell on nanoporous substrate, *J. Vac. Sci. Technol. A* 33 (2014) 01A145.
- [22] S. Ji, G.Y. Cho, W. Yu, P.-C. Su, M.H. Lee, S.W. Cha, Plasma-enhanced atomic layer deposition of nanoscale yttria-stabilized zirconia electrolyte for solid oxide fuel cells with porous substrate, *ACS Appl. Mater. Interfaces* 7 (2015) 2998.
- [23] J. An, Y.-B. Kim, F.B. Prinz, Ultra-thin platinum catalytic electrodes fabricated by atomic layer deposition, *Phys. Chem. Chem. Phys.* 15 (2013) 7520.
- [24] S.B. Adler, Factors governing oxygen reduction in solid oxide fuel cell cathodes, *Chem. Rev.* 104 (2004) 4791.
- [25] S. Ji, I. Chang, G.Y. Cho, Y.H. Lee, J.H. Shim, S.W. Cha, Application of dense nano-thin platinum films for low-temperature solid oxide fuel cells by atomic layer deposition, *Int. J. Hydrog. Energy* 39 (2014) 12402.
- [26] E.N. Armstrong, K.L. Duncan, D.J. Oh, J.F. Weaver, E.D. Wachsman, Determination of surface exchange coefficients of LSM, LSCF, YSZ, GDC constituent materials in composite SOFC cathodes, *J. Electrochem. Soc.* 158 (2011) B492.
- [27] W.C. Chueh, W. Lai, S.M. Haile, Electrochemical behavior of ceria with selected metal electrodes, *Solid State Ionics* 179 (2008) 1036.